Silicon SPAD monolithically integrated with SiON-based photonic circuit

Fabio Acerbi, Martino Bernard, Alberto Gola, Georg Pucker, Mher Ghulinyan
Fondazione Bruno Kessler – Sensors and Devices, via Sommarive 18, Trento, Italy
email: acerbi@fbk.eu, tel: +39 0461314158

INTRODUCTION

QUANTUM photonics represents one of the most fascinating fields of research. A generic quantum photonic system typically consists of generation, manipulation and detection of quantum states of light carried by single photons. In such a context, an important and hot-topic nowadays is the integration of single-photon detectors within the quantum PICs.

Among the technologies exploited for the implementation of single-photon detectors, the one operating at cryogenic temperatures, e.g. superconducting nanowire single photon detectors (SNSPDs), are now an established technology, reaching very high photon detection efficiency (PDE), >90%. Although integration of these detectors with waveguides has been demonstrated [1], these devices require a cryostat to operate at <4 K. On the contrary, going towards a fully integrated approach, CMOS compatibility is of prime importance. Some solutions have been proposed, for example, working in the SWIR range (e.g. at 1310 nm or 1550 nm) using a SOI photonic platform with Ge-on-Si based SPADs [2].

A different solution, with a better CMOS compatibility, is the use of silicon nitride (SiNx) or silicon oxynitride (SiON) based PIC platforms, operating with NIR photons (e.g. 850 nm). This can be realized on the top of a silicon chip, which include detectors and all ancillary electronics. In such kind of solutions, the main research topic nowadays is the efficient coupling between the optically transparent waveguide, where the light propagates inside the PIC, and the light-absorbing waveguide (or generically light-absorbing silicon region), where it is photo-detected.

PHOTONIC-ELECTRONIC INTEGRATED PLATFORM

In this paper we present a very efficient and fully CMOS compatible solution to realize a monolithic integration between SiON PICs fabricated on top of a silicon substrate, which include diodes and SPADs to detect the single-photons. The light coupling is based on the top-down convergence approach, where we shape the geometry of both the waveguide and the bottom cladding material [3][4]. The vertical cross-section at the SPAD location is shown in Fig. 1, whereas in Fig. 2 we report simulations of the light propagating in the waveguide (section A) and slowly exiting towards the SPAD sensitive region, with evanescent coupling, (sections B, C). This approach: i) uses CMOS compatible materials, ii) does not require alignments or butt-coupling, iii) operates at room temperature and iv) the design of the SPADs does not have particular constraints due to the PIC integration.

MEASUREMENTS

The SPAD layout is visible in Fig. 3. To characterize the performance of the PIC, we used the setup shown in Fig. 4: in particular, two inversely tapered fibers have been coupled to the input and output ports of the selected waveguide. The SPADs under test were connected to an external quenching and reset resistor, connected to a trans-impedance amplifier to acquire the avalanche signals with a 1 GHz bandwidth oscilloscope. The count rate has been measured with the inter-times histogram and described in [5]. The layout of the test chip is shown in

Fig. 5. We selected and tested some SPADs, in particular the ones coupled with the waveguide that pass through the highlighted in Fig. 5 Mach-Zehnder interferometer (MZI).

Measured primary noise (dark count rate, DCR) of SPADs T12 and T13 at different temperatures are shown in

Fig. 6. It is in the level of <100 cps at 20°C and almost doubles every 10°C. Statistically DCR spread on other SPADs is between few tens to few hundreds of cps. Fig. 7 shows the photon detection efficiency (PDE) of the same SPAD, at different wavelengths. This has been measured with external pulsed illumination, coming perpendicularly from the top. It peaks at about 570 nm, and it is ~25% at 850 nm, at 10 V excess bias.

We also measured the PDE of the waveguide+SPAD, in order to demonstrate the ability of the chip to detect the light injected in the waveguide from an attenuated external laser. Results are shown in Fig. 8. The comparison with PDE measured with light from the top allows to calculate the coupling efficiency of light from the waveguide to the SPAD, being 76-85%. Finally, we evaluated the count rate variation on the SPADs when modulating the light intensities by driving the MZI. As shown in Fig. 9, the light power is exchanged between the two waveguides, despite MZI does not achieve a full π-shift.

REFERENCES

[1] W.H.P. Pernice, et. al., "High-speed and high-efficiency travelling wave single-photon detectors embedded in nanophotonic circuits" Nature communications, 3, 1325, 2012, doi: 10.1038/ncomms2307

[2] N. J. D. Martinez, et. Al., "Single photon detection in a waveguide-coupled Ge-on-Si lateral avalanche photodiode", Optics Express, vol. 25, no. 14, Jul 2017, doi: 10.1364/OE.25.016130

[3] M. Bernard, et. al. "Top-down convergence of near-infrared photonics with silicon substrate-integrated electronics" Optica, vol. 8, no. 11, p. 1363, Nov. 2021, doi: 10.1364/OPTICA.441496

[4] M. Ghulinyan, M. Bernard, R. Bartali, and G. Pucker, "Formation of Mach angle profiles during wet etching of silica and silicon nitride materials", Appl. Surf. Sci. 359, 679 (2015).

[5] F. Acerbi, S. Gundacker, "Understanding and simulating SiPMs", Nucl Instrum Meth A, Vol., pp. 16-35, 2019, doi: 10.1016/j.nima.2018.11.118

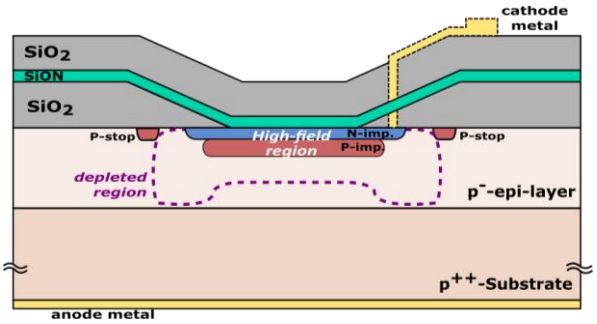

Fig. 1. Cross-section of the waveguide and the SPAD, in the coupling location. The bottom cladding material of the waveguide is etched and the waveguide lay on the silicon over the SPAD active area.

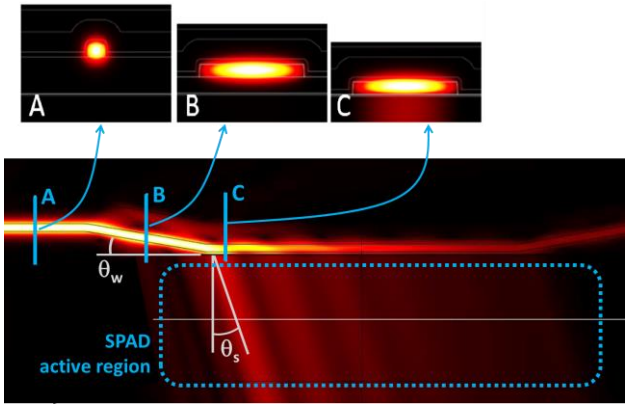

Fig. 2. Simulations of the field distribution in various regions of the waveguide: lateral view of the transition from the PIC to the detector region and the PIC cross-sections in different regions of interest.

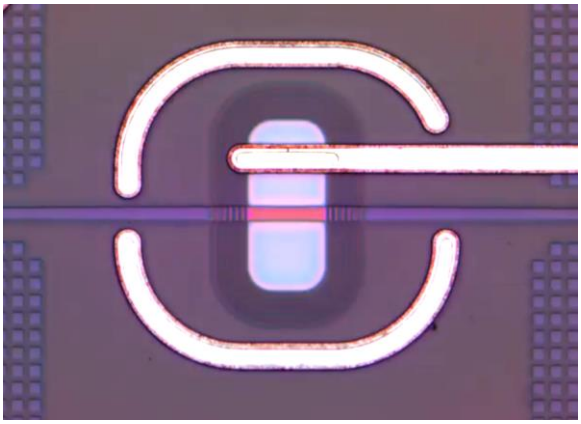

Fig. 3. Picture of the SPAD (from a newer production), showing the waveguides, the etched bottom cladding region and the metals for anode and cathode connections.

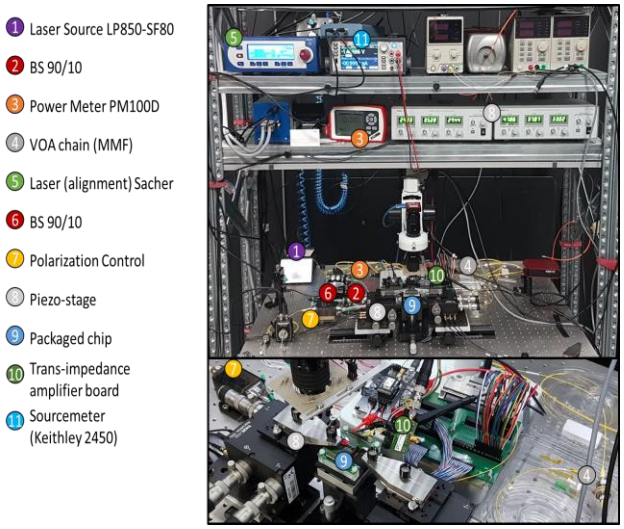

Fig. 4. Measurement setup used for PIC characterization

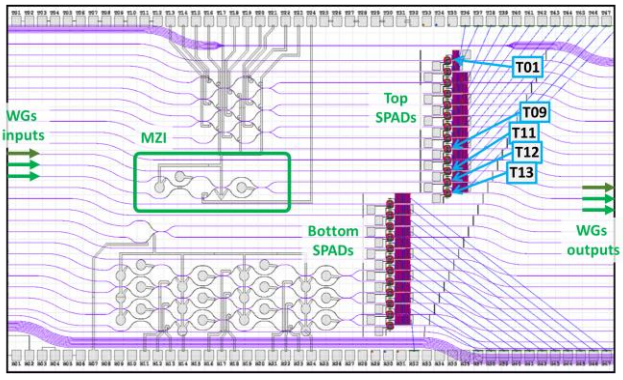

Fig. 5. Layout of the test chip, used to characterize the PIC with integrated single-photon detectors (SPADs)

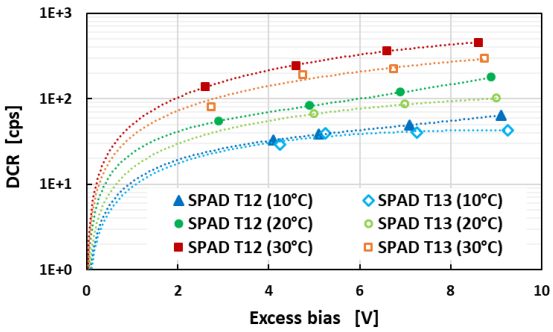

Fig. 6. Measured primary dark cunt rate (DCR) of the SPAD T12 and T13, at different temperatures, as a function of the excess bias.

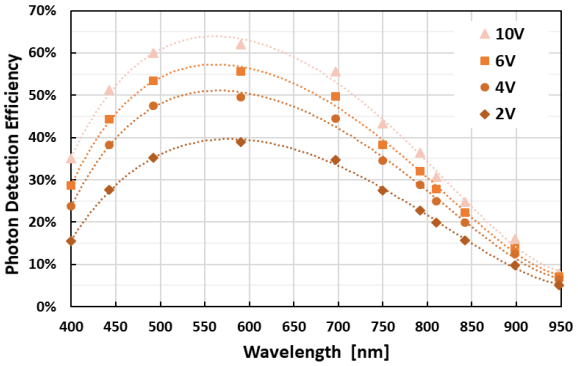

Fig. 7. Photon detection efficiency (PDE) of SPAD T12, measured at different wavelengths and excess biases, with illumination form the top (with pulsed LEDs).

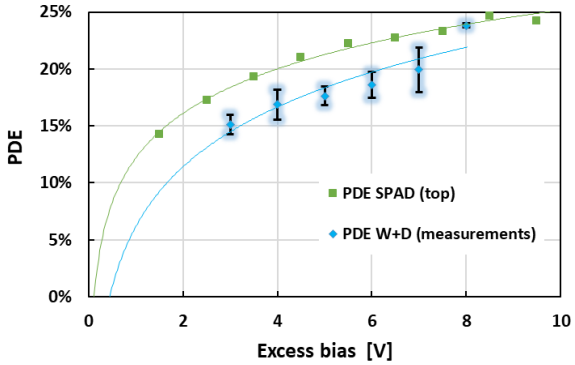

Fig. 8. Photon detection efficiency (PDE) of the waveguide+SPAD. It include the PDE of the SPAD and the coupling efficiency of light from the waveguide to the SPAD. Some SPADs have been measured and we report the average values and the variation between SPADs. By comparison the PDE of the SPAD alone, measured with top illumination.

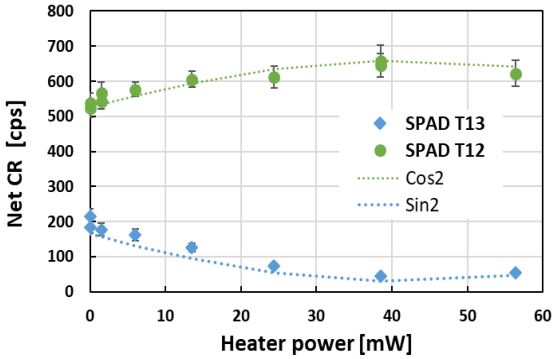

Fig. 9. Net count rate (with DCR subtracted), of SPAD T12 and T13, measured with light injected in one of the waveguide passing through the MZI, as a function of the driving power of one of the arms of the MZI.